Paper 222

©Civil-Comp Press, 2012
Proceedings of the Eleventh International Conference
on Computational Structures Technology,
B.H.V. Topping, (Editor),
Civil-Comp Press, Stirlingshire, Scotland

Multi-Patch Isogeometric Analysis of Space Rods

L. Greco and M. Cuomo
Dipartimento di Ingegneria Civile ed Ambientale
Università degli Studi di Catania, Italy

Abstract

This paper deals with the isogeometric analysis using B-splines of space rods subject to Kirchhoff-Love hypotheses. A multi-patch isogeometric approach for the numerical analysis of the three-dimensional Kirchhoff-Love rod theory is developed. We use Bezier and B-splines interpolations and we show that they are able to attain very good accuracy for rod structures, particularly for developing a three-dimensional exact curve element with geometric torsion. The patches in general present a C^n-continuity in the interior and are joined with C^0-continuity, so that the global tangent stiffness operator in general is singular. In order to avoid the singularity in the stiffness operator several continuity conditions at the joints of the patches are required. Either parametric or geometric continuity or can be imposed. In this work, we show how parametric continuity can be imposed by means of two additional constraints.

Keywords: B-spline continuity, Bezier interpolation, Kirchhoff-Love rod theory, curved elements.

1 Introduction

Structural models for curved space rods Model have been given by [1], [2], [3], in the context of Kirchhoff-Love hypotheses, and by [4], [5], for the Timoshenko model. Finite Element implementations of these models require special attention for the interpolation of the geometry, in order to guarantee the continuity of the intrinsic axes. In general, they exhibit jumps at the boundaries of the elements, that have to be smoothed in some way. In the context of standard polynomial interpolations many elements have been proposed for effectively treating this kind of structures, generally based on mixed or enhanced formulations [4],[5]. More recently, formulations that employ piecewise continuous interpolations on the elements have been proposed; the interelement con-

tinuity is imposed in a weak sense using the Discontinuous Galerkin approach [6].

Recently isogeometric analysis has gained more and more popularity in computational mechanics, and has been applied to many problems of solid and fluid mechanics. In isogeometric analysis B-splines interpolations are used, which guarantee C^{p-1} continuity, p being the degree of the spline, as opposite to the usual C^0 continuity obtained with the standard FEM discrete representations. The same interpolation is used for the degrees of freedom that define the deformed geometry, so that an isoparametric description is obtained. Although B-splines are not shape functions in the usual sense, they do verify the partition of unity.

Thanks to the high continuity properties, B-splines are very useful for beams and shells, since they can incorporate in the analysis the initial geometric curvatures without discontinuities. Isogeometric analysis of shell models has been used in [7] for polar and in [8] and [9] for non polar shells. In [10] a procedure for joining different patches under Kirchhoff-Love hypotheses is proposed.

In the field of 1D structural theories rod models have been developed on the basis of the theory of Simo [11]. References [12], [13] are relative to polar beams. Timoshenko rod models are more common than Kirchhoff-Love model for finite deformation space rods, since the continuity conditions for rotations are automatically imposed within a C^0 continuity. However, the Kirchhoff-Love model has the advantage of avoiding shear locking phenomena that are crritical for slender elements.

In a recent paper [14] a pure displacement finite deformation *B-Spline* isoparametric formulation of a space rod model based on the Kirchhoff-Love model has been proposed. A parametrization of the cross section independent from the *Frenet*'s triad was introduced. The normal vectors attached to the centroid curve are mapped by a correction angle, ϕ, that coincides with the torsional twist. The geometry of the axis is defined via a uniform collocation of the control points. The tangent and normal vectors are defined on the interpolation of the geometry. One patch was used for the entire beam. The numerical implementation resulted very effective, with convergence rate equal to the degree of the interpolation, thanks to the fact that the model is only based on displacements.

In the paper it is presented an extension of the formulation to multipatch space rods. Although in general a single patch can be used for modeling a rod, and degrees of freedom can be added increasing the number of internal knots, there are cases when it is necessary to discretise the beam with more than one patch. important examples are reticulated and framed structures, composed by rods that are connected at the ends by rigid links requiring that the tangents keep their relative orientation during the deformation. Also in the cases of beams with sharply varying cross sections it may be useful the use of multiple path interpolations.

The patches in general present C^{p-1} continuity in the interior and are joined with C^0 continuity, so that the global tangent stiffness operator in general is singular. In order to avoid the singularity in the stiffness operator several continuity conditions at the joints of the patches are required. Either parametric continuity (C^1 or C^2) or geometric continuity (G^1 or G^2) conditions can be imposed.

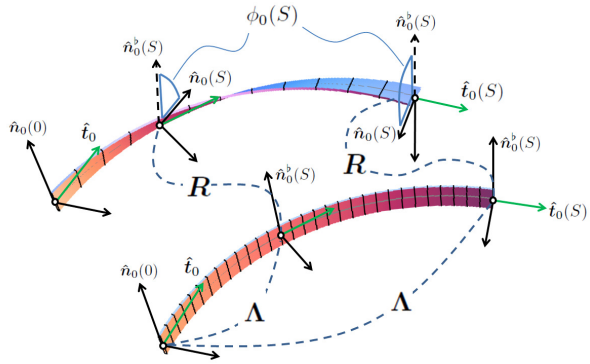

Figure 1: Intrinsic reference axes on the initial geometry of the rod

The geometric continuity conditions are weaker than the parametric conditions. The continuity conditions in the CAD -literature are known as the β-constraints and represent constraint conditions for the positions of the control points where the scalar β-quantity represents additional unknowns [9]. In this work, we don't impose the continuity conditions via β-constraints but directly by means of the Lagrange multipliers method.

2 Space rod model

In this section it is given a short summary of the Kirchhoff-Love space rod model described in [14]. The rod is defined by a pair $\mathcal{A}, \hat{\boldsymbol{n}}$ where $\mathcal{A} =]0, L_0[$ is an open set of $\mathbb{R}$, that is the parametric domain of the curve $\boldsymbol{P}(S) : \mathcal{A} \to \mathbb{R}^3$ and $\hat{\boldsymbol{n}}_0(S) : \mathcal{A} \to \mathbb{R}^3$ is a unit vector field everywhere orthogonal to that curve. An index '0' denotes the initial undeformed configuration. The arc-length along the original rod axis id indicated by S. The tangent vector to the reference configuration of the curve is then the unit vector field $\hat{\boldsymbol{t}}_0 : \mathcal{A} \to \mathbb{R}^3$ with $\hat{\boldsymbol{t}}_0 = \frac{d\boldsymbol{p}_0}{dS}$ (a hat indicates a unit vector).

The orientation of the normal vector $\hat{\boldsymbol{n}}_0$ to the beam is obtained by means of the combination of two rotations. The first, Λ, is the rotation around $\hat{\boldsymbol{t}}_0(0)$ that transforms $\hat{\boldsymbol{t}}_0(0)$ in $\hat{\boldsymbol{t}}_0(S)$ without drilling rotation, and is totally defined by the curve geometry. The second is a pure torsional rotation ϕ_0 around the unit tangent $\hat{\boldsymbol{t}}_0(S)$, so that

$$\hat{\boldsymbol{n}}_0(S) = \boldsymbol{R}(\hat{\boldsymbol{t}}_0(S), \phi_0(S))\hat{\boldsymbol{n}}_0^\flat(S) = \boldsymbol{R}(\hat{\boldsymbol{t}}_0(S), \phi_0(S))\boldsymbol{\Lambda}(\hat{\boldsymbol{t}}_0(0), \hat{\boldsymbol{t}}_0(S))\, \hat{\boldsymbol{n}}_0(0). \quad (1)$$

The unit local triad is completed by the unit vector

$$\hat{\boldsymbol{\nu}}_0(S) = \hat{\boldsymbol{t}}_0(S) \times \hat{\boldsymbol{n}}_0(S) \quad (2)$$

The space rod is thus defined by the position vector $\boldsymbol{p}_0(S)$ and by the initial twist angle $\phi_0(S)$. (see figure 1).

2.1 Kinematics of the Kirchhoff Love rod

The current centroid curve is indicated by $\boldsymbol{p}(S) : [0, L_0] \to \mathbb{R}^3$ and is given by

$$\boldsymbol{p}(S) = \boldsymbol{p}_0(S) + \boldsymbol{u}(S), \tag{3}$$

The Lagrangian arc-length parametrization of the current tangent vector field $\boldsymbol{t}(S)$ is

$$\hat{\boldsymbol{t}}(S) = \frac{\boldsymbol{t}(S)}{\|\boldsymbol{t}(S)\|} = \frac{1}{\|\boldsymbol{t}(S)\|}\frac{d\boldsymbol{p}}{dS}. \tag{4}$$

The rotation of the cross section is given by two isometric operators, $\boldsymbol{\Lambda}(\hat{\boldsymbol{t}}_0(S), \hat{\boldsymbol{t}}(S))$, a rotation without drilling rotation around the vector $\hat{\boldsymbol{t}}_0(S)$, and $\boldsymbol{R}(\hat{\boldsymbol{t}}(S), \phi(S))$ that gives the drilling rotation $\phi(S) : [0, L_0] \to \mathbb{R}$ around the vector $\hat{\boldsymbol{t}}(S)$. The two operators are obtained particularizing *Euler-Rodriguez* formula

$$\mathtt{R} = \hat{\boldsymbol{e}} \otimes \hat{\boldsymbol{e}} + \cos[\varphi](\boldsymbol{I} - \hat{\boldsymbol{e}} \otimes \hat{\boldsymbol{e}}) + \sin[\varphi]\hat{\boldsymbol{e}} \times \boldsymbol{I}. \tag{5}$$

The unitary axial vector of the first rotation is $\hat{\boldsymbol{e}} = \frac{\hat{\boldsymbol{t}}_0 \times \hat{\boldsymbol{t}}}{\|\hat{\boldsymbol{t}}_0 \times \hat{\boldsymbol{t}}\|}$ while $\cos[\varphi] = \hat{\boldsymbol{t}}_0 \cdot \hat{\boldsymbol{t}}$ and $\sin[\varphi] = \|\hat{\boldsymbol{t}}_0 \times \hat{\boldsymbol{t}}\|$, therefore the formula (5) gives the representation

$$\boldsymbol{\Lambda}(\hat{\boldsymbol{t}}_0, \hat{\boldsymbol{t}}) = (\hat{\boldsymbol{t}}_0 \cdot \hat{\boldsymbol{t}})\boldsymbol{I} + [\hat{\boldsymbol{t}}_0 \times \hat{\boldsymbol{t}}] \times \boldsymbol{I} + \frac{1}{1 + \hat{\boldsymbol{t}}_0 \cdot \hat{\boldsymbol{t}}}(\hat{\boldsymbol{t}}_0 \times \hat{\boldsymbol{t}}) \otimes (\hat{\boldsymbol{t}}_0 \times \hat{\boldsymbol{t}}) \tag{6}$$

.

The axial vector of the second rotation operator is $\hat{\boldsymbol{e}} = \hat{\boldsymbol{t}}$. Setting $\varphi = \phi$ and using the properties of the double cross product: the Rodriguez operator (5) assumes the form

$$\boldsymbol{R}(\hat{\boldsymbol{t}}, \phi) = \boldsymbol{I} + \sin[\phi]\, \hat{\boldsymbol{t}} \times \boldsymbol{I} + (1 - \cos[\phi])\, \hat{\boldsymbol{t}} \times [\hat{\boldsymbol{t}} \times \boldsymbol{I}]. \tag{7}$$

.

The Lagrangian parametrization of the current directors $\hat{\boldsymbol{n}}(S)$ and $\hat{\boldsymbol{\nu}}(S)$ are then

$$\hat{\boldsymbol{n}}(S) = \boldsymbol{R}(\hat{\boldsymbol{t}}, \phi)\boldsymbol{\Lambda}(\hat{\boldsymbol{t}}_0, \hat{\boldsymbol{t}})\hat{\boldsymbol{n}}_0(S), \quad \hat{\boldsymbol{\nu}}(S) = \boldsymbol{R}(\hat{\boldsymbol{t}}, \phi)\boldsymbol{\Lambda}(\hat{\boldsymbol{t}}_0, \hat{\boldsymbol{t}})\hat{\boldsymbol{\nu}}_0(S). \tag{8}$$

The construction described satisfies Kirchhoff-Love hypotheses $\hat{\boldsymbol{t}} \cdot \hat{\boldsymbol{n}} = \hat{\boldsymbol{t}} \cdot \hat{\boldsymbol{\nu}} = 0$. We observe that the Lagrangian description of the internal state of the rod is defined by means of the two field $\{\boldsymbol{u}(S), \phi(S)\}$, so that it has four degrees of freedom. Introducing the Lagrangian coordinates along the normal axes, the position of a generic point in the cross section is identified by the vector

$$\overset{*}{\boldsymbol{p}}(S, \vartheta^n, \vartheta^\nu) = \boldsymbol{p}(S) + \boldsymbol{\xi} = \boldsymbol{p}(S) + \vartheta^n \hat{\boldsymbol{n}}(S) + \vartheta^\nu \hat{\boldsymbol{\nu}}(S). \tag{9}$$

The tangent vectors at the generic fibre of the rod are obtained differentiating equation (9)

$$\overset{*}{\boldsymbol{t}} := \frac{\partial \overset{*}{\boldsymbol{p}}}{\partial S} = \frac{\partial \boldsymbol{p}}{\partial S} + \vartheta^{\nu}\frac{\partial \hat{\boldsymbol{\nu}}}{\partial S} + \vartheta^{n}\frac{\partial \hat{\boldsymbol{n}}}{\partial S}, \quad \overset{*}{\boldsymbol{n}} := \frac{\partial \overset{*}{\boldsymbol{p}}}{\partial \vartheta^{n}} = \hat{\boldsymbol{n}}, \quad \overset{*}{\boldsymbol{\nu}} := \frac{\partial \overset{*}{\boldsymbol{p}}}{\partial \vartheta^{\nu}} = \hat{\boldsymbol{\nu}} \tag{10}$$

By means of equations (10) we define the push forward operator from the centroid line of the rod to the generic fibre,

$$\boldsymbol{z} = \overset{*}{\boldsymbol{g}}_{\alpha} \otimes \boldsymbol{g}^{\natural\alpha},\ \overset{*}{\boldsymbol{g}}_{\alpha} = \{\overset{*}{\boldsymbol{t}}, \hat{\boldsymbol{n}}, \hat{\boldsymbol{\nu}}\},\ \boldsymbol{g}_{\alpha} = \{\boldsymbol{t}, \hat{\boldsymbol{n}}, \hat{\boldsymbol{\nu}}\} \tag{11}$$

and the index $\natural$ indicates the contravariant base vectors.

In order to simplify the notations, it is useful to introduce the definitions of the geometric curvatures of the beam in a generic configuration, $\frac{1}{R_n} = \frac{1}{\|\boldsymbol{t}\|}\frac{d\hat{\boldsymbol{n}}}{dS} \cdot \hat{\boldsymbol{t}}$, $\frac{1}{R_\nu} = \frac{1}{\|\boldsymbol{t}\|}\frac{d\hat{\boldsymbol{\nu}}}{dS} \cdot \hat{\boldsymbol{t}}$, $\frac{1}{\tau} = \frac{1}{\|\boldsymbol{t}\|}\frac{d\hat{\boldsymbol{n}}}{dS} \cdot \hat{\boldsymbol{\nu}}$. The latter is the torsional curvature. Note that in a non geodetic rod it is

$$\hat{\boldsymbol{n}} \cdot \overset{*}{\boldsymbol{t}} = -\frac{\vartheta^{\nu}}{\tau}, \quad \hat{\boldsymbol{\nu}} \cdot \overset{*}{\boldsymbol{t}} = \frac{\vartheta^{n}}{\tau} \tag{12}$$

2.2 Tangent operator

The internal tangent operator and the velocity of deformation tensors are derived in detail in [14]. For the sake of completeness we summarize the main results.

The velocity of a generic point of the beam is

$$\dot{\overset{*}{\boldsymbol{p}}} = \dot{\boldsymbol{u}} + \vartheta^{n}\dot{\hat{\boldsymbol{n}}} + \vartheta^{\nu}\dot{\hat{\boldsymbol{\nu}}} \tag{13}$$

so that it is necessary to characterize the motion of the intrinsic triad. Since

$$\{\hat{\boldsymbol{t}}, \hat{\boldsymbol{n}}, \hat{\boldsymbol{\nu}}\} = \boldsymbol{Q}\{\hat{\boldsymbol{t}}_0, \hat{\boldsymbol{n}}_0, \hat{\boldsymbol{\nu}}_0\} \Rightarrow \{\dot{\hat{\boldsymbol{t}}}, \dot{\hat{\boldsymbol{n}}}, \dot{\hat{\boldsymbol{\nu}}}\} = \dot{\boldsymbol{Q}}\{\hat{\boldsymbol{t}}_0, \hat{\boldsymbol{n}}_0, \hat{\boldsymbol{\nu}}_0\} = \dot{\boldsymbol{Q}}\boldsymbol{Q}^{-1}\{\hat{\boldsymbol{t}}, \hat{\boldsymbol{n}}, \hat{\boldsymbol{\nu}}\} \tag{14}$$

it is necessary to evaluate the variation of the unit $\boldsymbol{Q}$-operator. It is possible to prove that [14]

$$\dot{\boldsymbol{Q}} = \dot{\boldsymbol{\Lambda}} + \dot{\boldsymbol{R}} = \left(\dot{\hat{\boldsymbol{t}}} \otimes \hat{\boldsymbol{t}} - \hat{\boldsymbol{t}} \otimes \dot{\hat{\boldsymbol{t}}}\right) + \dot{\phi}\,\hat{\boldsymbol{t}} \times \boldsymbol{I}. \tag{15}$$

The spin vector $\boldsymbol{\omega}(S) : [0, L_0] \to \mathbb{R}^3$ associated to $\dot{\boldsymbol{Q}}$ is:

$$\boldsymbol{\omega} = \dot{\phi}\hat{\boldsymbol{t}} + \omega_n\hat{\boldsymbol{n}} + \omega_\nu\hat{\boldsymbol{\nu}} \tag{16}$$

with

$$\omega_n = \dot{\hat{\boldsymbol{\nu}}} \cdot \hat{\boldsymbol{t}} = -\frac{1}{\|\boldsymbol{t}\|}\frac{d\dot{\boldsymbol{u}}}{dS} \cdot \hat{\boldsymbol{\nu}}; \quad \omega_\nu = -\dot{\hat{\boldsymbol{n}}} \cdot \hat{\boldsymbol{t}} = \frac{1}{\|\boldsymbol{t}\|}\frac{d\dot{\boldsymbol{u}}}{dS} \cdot \hat{\boldsymbol{n}}. \tag{17}$$

With the aid of the rotation vector $\boldsymbol{\omega}$, the velocity of the intrinsic triad takes the form

$$\begin{aligned}
\dot{\hat{\boldsymbol{t}}} &= \omega_\nu \hat{\boldsymbol{n}} - \omega_n \hat{\boldsymbol{\nu}} \\
\dot{\hat{\boldsymbol{n}}} &= -\omega_\nu \hat{\boldsymbol{t}} + \dot{\phi} \hat{\boldsymbol{\nu}} \\
\dot{\hat{\boldsymbol{\nu}}} &= \omega_n \hat{\boldsymbol{t}} - \dot{\phi} \hat{\boldsymbol{n}}.
\end{aligned} \tag{18}$$

We observe, for later use, that the continuity of the beam is guaranteed if the velocities of the torsional rotation $\dot{\phi}$ and of the bending rotations ω_n, ω_ν are continuous. In particular, the continuity of the bending rotations requires the continuity of the norm $\|\boldsymbol{t}\|$ of the tangent vector, and the continuity of the normal components of the line gradient of the velocity.

The derivative along the arc length of $\boldsymbol{\omega}$ is the curvature vector

$$\frac{1}{\|\boldsymbol{t}\|}\frac{d\boldsymbol{\omega}}{dS} = \dot{\chi}_t \hat{\boldsymbol{t}} + \dot{\chi}_n \hat{\boldsymbol{n}} + \dot{\chi}_\nu \hat{\boldsymbol{\nu}} \tag{19}$$

$$\begin{aligned}
\dot{\chi}_t &= \frac{1}{\|\boldsymbol{t}\|}\frac{d\dot{\phi}}{dS} + \frac{\omega_n}{R_n} + \frac{\omega_\nu}{R_\nu} \\
\dot{\chi}_n &= \frac{1}{\|\boldsymbol{t}\|}\frac{d\omega_n}{dS} - \frac{\omega_\nu}{\tau} - \frac{\dot{\phi}}{R_n} \\
\dot{\chi}_\nu &= \frac{1}{\|\boldsymbol{t}\|}\frac{d\omega_\nu}{dS} + \frac{\omega_n}{\tau} - \frac{\dot{\phi}}{R_\nu}.
\end{aligned} \tag{20}$$

The bending velocity of curvature can be related to the second covariant derivative of the velocity of displacement vector, $\frac{1}{\|\boldsymbol{t}\|^2}\frac{d^2\dot{\boldsymbol{u}}}{dS^2} = \frac{1}{\|\boldsymbol{t}\|}\frac{d}{dS}\left(\frac{1}{\|\boldsymbol{t}\|}\frac{d\dot{\boldsymbol{u}}}{dS}\right)$, in the form

$$\begin{aligned}
\dot{\chi}_n &= -\frac{1}{\|\boldsymbol{t}\|^2}\frac{d^2\dot{\boldsymbol{u}}}{dS^2}\cdot\hat{\boldsymbol{\nu}} - \frac{\dot{\phi}}{R_n} - \frac{1}{\|\boldsymbol{t}\|^2}\dot{\boldsymbol{t}}\cdot\boldsymbol{t}\frac{1}{R_\nu} \\
\dot{\chi}_\nu &= \frac{1}{\|\boldsymbol{t}\|^2}\frac{d^2\dot{\boldsymbol{u}}}{dS^2}\cdot\hat{\boldsymbol{n}} - \frac{\dot{\phi}}{R_\nu} + \frac{1}{\|\boldsymbol{t}\|^2}\dot{\boldsymbol{t}}\cdot\boldsymbol{t}\frac{1}{R_n}.
\end{aligned} \tag{21}$$

2.3 The velocity of deformation operator for a Kirchhoff-Love rod

Denoting with $\boldsymbol{F}$ the gradient of deformation from the reference configuration of the axis to its current configuration i.e. $\boldsymbol{F} = \boldsymbol{g}_\alpha \otimes \boldsymbol{g}^{\natural\alpha} = \boldsymbol{t} \otimes \boldsymbol{t}_0 + \hat{\boldsymbol{n}} \otimes \hat{\boldsymbol{n}} + \hat{\boldsymbol{\nu}} \otimes \hat{\boldsymbol{\nu}}$ and with $\overset{*}{G} = \overset{*}{\boldsymbol{g}}_\alpha \otimes \overset{*}{\boldsymbol{g}}^{\natural\alpha} = \overset{*}{\boldsymbol{t}} \otimes \overset{*}{\boldsymbol{t}}^{\natural} + \hat{\boldsymbol{n}} \otimes \overset{*}{\boldsymbol{n}}^{\natural} + \boldsymbol{\nu} \otimes \overset{*}{\boldsymbol{\nu}}^{\natural}$ the metric tensor at the generic fibre, its pull back on the centroid axis of the reference configuration is $\psi^*(\overset{*}{G}) =$

$\boldsymbol{F}^T \boldsymbol{z}^T \overset{*}{G} \boldsymbol{z} \boldsymbol{F}$, whose components on the triad $\hat{\boldsymbol{t}}_0, \hat{\boldsymbol{n}}_0, \hat{\boldsymbol{\nu}}_0$, after enforcing the Kirchhoff-Love constraints, and using expressions (12), are

$$\begin{pmatrix} \overset{*}{\boldsymbol{t}} \cdot \overset{*}{\boldsymbol{t}} & -\frac{\vartheta^\nu}{\tau}\|\boldsymbol{t}\| & \frac{\vartheta^n}{\tau}\|\boldsymbol{t}\| \\ -\frac{\vartheta^\nu}{\tau}\|\boldsymbol{t}\| & 1 & 0 \\ \frac{\vartheta^n}{\tau}\|\boldsymbol{t}\| & 0 & 1 \end{pmatrix} \tag{22}$$

The pull-back of the velocity of deformation on the reference configuration $\dot{\boldsymbol{E}} = \dot{E}_{\alpha\beta} \boldsymbol{g}_0^{\natural\alpha} \otimes \boldsymbol{g}_0^{\natural}\beta = sym\left((\boldsymbol{z}\boldsymbol{F})^T \dot{\overline{\boldsymbol{z}\boldsymbol{F}}}\right)$ has the components

$$\dot{\boldsymbol{E}} = \frac{1}{2}\begin{pmatrix} 2\,\dot{\overset{*}{\boldsymbol{t}}} \cdot \overset{*}{\boldsymbol{t}} & -\vartheta^\nu\left(\frac{d\dot{\hat{\boldsymbol{n}}}}{dS}\cdot\hat{\boldsymbol{\nu}} + \frac{d\hat{\boldsymbol{n}}}{dS}\cdot\dot{\hat{\boldsymbol{\nu}}}\right) & \vartheta^n\left(\frac{d\dot{\hat{\boldsymbol{n}}}}{dS}\cdot\hat{\boldsymbol{\nu}} + \frac{d\hat{\boldsymbol{n}}}{dS}\cdot\dot{\hat{\boldsymbol{\nu}}}\right) \\ -\vartheta^\nu\left(\frac{d\dot{\hat{\boldsymbol{n}}}}{dS}\cdot\hat{\boldsymbol{\nu}} + \frac{d\hat{\boldsymbol{n}}}{dS}\cdot\dot{\hat{\boldsymbol{\nu}}}\right) & 0 & 0 \\ \vartheta^n\left(\frac{d\dot{\hat{\boldsymbol{n}}}}{dS}\cdot\hat{\boldsymbol{\nu}} + \frac{d\hat{\boldsymbol{n}}}{dS}\cdot\dot{\hat{\boldsymbol{\nu}}}\right) & 0 & 0 \end{pmatrix} \tag{23}$$

The components of the velocity of deformation are readily found performing the derivatives in (23). The components of the shear deformation velocity are given by the off-diagonal terms of tensor (23). Since

$$\left(\frac{d\dot{\hat{\boldsymbol{n}}}}{dS}\cdot\hat{\boldsymbol{\nu}} + \frac{d\hat{\boldsymbol{n}}}{dS}\cdot\dot{\hat{\boldsymbol{\nu}}}\right) = \frac{1}{\|\boldsymbol{t}\|}\frac{d\dot{\phi}}{dS} + \frac{\omega_n}{R_n} + \frac{\omega_\nu}{R_\nu} = \dot{\chi}_t \tag{24}$$

one has

$$\dot{\gamma}_{\hat{n}\overset{*}{t}} = -\vartheta^\nu \dot{\chi}_t \quad \dot{\gamma}_{\hat{\nu}\overset{*}{t}} = \vartheta^n \dot{\chi}_t \tag{25}$$

The result (20) and definitions (17) and the identity

$$\hat{\boldsymbol{t}} \times \frac{d\hat{\boldsymbol{t}}}{dS} = \|\boldsymbol{t}\|\left(-\frac{\hat{\boldsymbol{n}}}{R_\nu} + \frac{\hat{\boldsymbol{\nu}}}{R_n}\right) \tag{26}$$

allow to get a representation of $\dot{\chi}_t$ in terms of the Lagrangian generalized velocity vector $\dot{\boldsymbol{q}} = \{\dot{\boldsymbol{u}}, \dot{\phi}\}$:

$$\dot{\chi}_t = \frac{1}{\|\boldsymbol{t}\|}\left(\hat{\boldsymbol{t}} \times \frac{d\hat{\boldsymbol{t}}}{dS}\right)\cdot\frac{d\dot{\boldsymbol{u}}}{dS} + \frac{d\dot{\phi}}{dS}. \tag{27}$$

Using expression (10) and disregarding the terms quadratic in the normal coordinates, the Lagrangian axial deformation of the generic fibre can be written as

$$\overset{*}{\boldsymbol{t}} \cdot \overset{*}{\boldsymbol{t}} \approx \boldsymbol{t}\cdot\boldsymbol{t} + 2\|\boldsymbol{t}\|^2\frac{\vartheta^n}{R_n} + 2\|\boldsymbol{t}\|^2\frac{\vartheta^\nu}{R_\nu} \tag{28}$$

The axial velocity is then given by

$$
\begin{aligned}
\dot{\overset{*}{\boldsymbol{t}}} \cdot \overset{*}{\boldsymbol{t}} = \dot{\boldsymbol{t}} \cdot \boldsymbol{t} + \vartheta^n \left(-\frac{d\omega_\nu}{dS}\|\boldsymbol{t}\| + \frac{\dot{\phi}}{R_\nu}\|\boldsymbol{t}\|^2 - \frac{\omega_n}{\tau}\|\boldsymbol{t}\| + \frac{\dot{\boldsymbol{t}} \cdot \boldsymbol{t}}{R_n} \right) \\
+ \vartheta^\nu \left(\frac{d\omega_n}{dS}\|\boldsymbol{t}\| - \frac{\dot{\phi}}{R_n}\|\boldsymbol{t}\|^2 - \frac{\omega_\nu}{\tau}\|\boldsymbol{t}\| + \frac{\dot{\boldsymbol{t}} \cdot \boldsymbol{t}}{R_\nu} \right)
\end{aligned} \tag{29}
$$

that can be cast in the form:

$$
\dot{\overset{*}{\boldsymbol{t}}} \cdot \overset{*}{\boldsymbol{t}} = \dot{\varepsilon}_r + \dot{\boldsymbol{\chi}}^\perp \cdot \boldsymbol{\xi}\|\boldsymbol{t}\| \tag{30}
$$

with the notations

$$
\begin{aligned}
\dot{\varepsilon}_r &= \dot{\boldsymbol{t}} \cdot \boldsymbol{t} \left(1 + \frac{\theta^n}{R_n} + \frac{\theta^\nu}{R_\nu} \right) = \dot{\boldsymbol{t}} \cdot \boldsymbol{t} \left(1 - \boldsymbol{\xi} \cdot \frac{d\hat{\boldsymbol{t}}}{dS} \frac{1}{\|\boldsymbol{t}\|} \right) \\
\dot{\boldsymbol{\chi}}^\perp &= \hat{\boldsymbol{t}} \times \dot{\boldsymbol{\chi}} \\
\boldsymbol{\xi} &= \theta_n \hat{\boldsymbol{n}} + \theta_\nu \hat{\boldsymbol{\nu}}
\end{aligned} \tag{31}
$$

An alternative expression for the axial velocity of deformation, using equation (21) is

$$
\begin{aligned}
\dot{\overset{*}{\boldsymbol{t}}} \cdot \overset{*}{\boldsymbol{t}} &= \dot{\varepsilon} + \boldsymbol{\xi} \cdot \dot{\boldsymbol{\chi}_{\boldsymbol{r}}}^\perp \|\boldsymbol{t}\| \\
\dot{\varepsilon} = \dot{\boldsymbol{t}} \cdot \boldsymbol{t} \quad \|\boldsymbol{t}\| \dot{\boldsymbol{\chi}_{\boldsymbol{r}}}^\perp &= -\frac{d^2 \dot{\boldsymbol{u}}}{dS^2} + \left(\hat{\boldsymbol{t}} \times \frac{d\boldsymbol{t}}{dS} \right) \|\boldsymbol{t}\| \dot{\phi}.
\end{aligned} \tag{32}
$$

3 Equilibrium operator for *Kirchhoff-Love* rod

3.1 Virtual Power Identity

The equilibrium operator is obtained from the principle of virtual power. The representation of the internal power on the reference configuration is:

$$
P_{int} = \int_{L_0} \left(\int_{\mathcal{A}} \boldsymbol{S} : \dot{\boldsymbol{E}} \, d\mathcal{A} \right) dS, \tag{33}
$$

with $\boldsymbol{S} = S^{\alpha\beta} \boldsymbol{g}_{0\alpha} \otimes \boldsymbol{g}_{0\beta}$ the second Piola-Kirchhoff stress tensor, given by

$$
\boldsymbol{S} = \det(\boldsymbol{z}\boldsymbol{F})(\boldsymbol{z}\boldsymbol{F})^{-1} \overset{*}{\boldsymbol{\Sigma}} (\boldsymbol{z}\boldsymbol{F})^{-T} \tag{34}
$$

Its components on the reference unitary centroid triads are

$$
S = \begin{pmatrix} S^{tt} & S^{tn} & S^{t\nu} \\ S^{nt} & 0 & 0 \\ S^{\nu t} & 0 & 0 \end{pmatrix}. \tag{35}
$$

Substituting the components of the velocity of deformation, one has

$$
\begin{aligned}
P_{int} &= \int_{L_0} \left(\int_{\mathcal{A}} S^{tt}(\dot{\varepsilon} - \vartheta^n \dot{\chi}_\nu \|\boldsymbol{t}\| + \vartheta^\nu \dot{\chi}_n)\|\boldsymbol{t}\| + (S^{\nu t}\vartheta^n - S^{nt}\vartheta^\nu)\dot{\chi}_t \, d\mathcal{A} \right) dS \\
&= \int_{L_0} (N\dot{\varepsilon} + \boldsymbol{M} \cdot \dot{\boldsymbol{\chi}}_r \|\boldsymbol{t}\| + M_t \dot{\chi}_t) \, dS \\
&= \int_{L_0} \left(N \left(\frac{d\dot{\boldsymbol{u}}}{dS} \cdot \boldsymbol{t} \right) + M_n \left(-\frac{d^2\dot{\boldsymbol{u}}}{dS^2} \cdot \hat{\boldsymbol{\nu}} - \frac{\|\boldsymbol{t}\|^2}{R_n}\dot{\phi} \right) \right) + \\
&\quad M_\nu \left(\frac{d^2\dot{\boldsymbol{u}}}{dS^2} \cdot \hat{\boldsymbol{n}} - \frac{\|\boldsymbol{t}\|^2}{R_\nu}\dot{\phi} \right) + M_t \left(\frac{d\dot{\phi}}{dS} + \frac{1}{\|\boldsymbol{t}\|}\frac{d\dot{\boldsymbol{u}}}{dS} \left(\hat{\boldsymbol{t}} \times \frac{d\hat{\boldsymbol{t}}}{dS} \right) \right) dS,
\end{aligned}
\tag{36}
$$

where the following definitions have been introduced:

$$
\begin{aligned}
N &= \int_{\mathcal{A}} S^{tt} d\mathcal{A}, \\
\boldsymbol{M} &= \int_{\mathcal{A}} \boldsymbol{\xi} \times (S^{tt}\hat{\boldsymbol{t}}) \, d\mathcal{A}, \\
M_t &= \int_{\mathcal{A}} (S^{\nu t}\vartheta^n - S^{nt}\vartheta^\nu) \, d\mathcal{A}.
\end{aligned}
\tag{37}
$$

3.2 Constitutive operator of the rod

We assume that the rod remains elastic, and denote by

$$
\dot{\boldsymbol{S}} = \mathbb{C}_t : \dot{\boldsymbol{E}} \tag{38}
$$

the tangent constitutive relationship between the increment of the second Piola-Kirchhoff stress tensor and the convective velocity of deformation. In this work we employ the approximation that the tangent elastic coefficients be constant, and according to [11], [10], we assume that

$$
\begin{aligned}
\dot{S}^{tt} &= E\,(\dot{\overset{*}{\boldsymbol{t}}} \cdot \overset{*}{\boldsymbol{t}}) = \mathcal{E}\left[\dot{\varepsilon}\left(1 + \frac{\vartheta^n}{R_n} + \frac{\vartheta^\nu}{R_\nu} \right) - \vartheta^n \dot{\chi}_\nu \|\boldsymbol{t}\| + \vartheta^\nu \dot{\chi}_n \|\boldsymbol{t}\| \right] \\
&= E\left[\dot{\boldsymbol{t}} \cdot \boldsymbol{t} + \vartheta^n \left(-\frac{d^2\dot{\boldsymbol{u}}}{dS^2} \cdot \hat{\boldsymbol{n}} + \|\boldsymbol{t}\|^2 \frac{\dot{\phi}}{R_\nu} \right) + \vartheta^\nu \left(-\frac{d^2\dot{\boldsymbol{u}}}{dS^2} \cdot \hat{\boldsymbol{\nu}} - \|\boldsymbol{t}\|^2 \frac{\dot{\phi}}{R_n} \right) \right] \\
\dot{S}^{tn} &= -G\,\vartheta^\nu\,\dot{\chi}_t \quad \dot{S}^{t\nu} = G\,\vartheta^n\,\dot{\chi}_t.
\end{aligned}
\tag{39}
$$

4 Numerical Formulation

4.1 B-Spline interpolation

A B-Spline curve of degree p is defined as

$$\mathbf{C}(\lambda) = \sum_{i=1}^{n} N_{i,p}(\lambda)\mathbf{P}_i \tag{40}$$

where $\mathbf{P}_i = \{P_{ix}, P_{iy}, P_{iz}\}$ are the cartesian components of n control points, and $N_{i,p}$ are the n B-Spline basis functions of degree p defined on a non periodic knot vector. The knot vector is a non decreasing sequence of m real numbers, the parametric coordinate $\lambda_j, j = 1, ..., m$, with $m = n + p + 1$,

$$\Xi = \{\underbrace{a, ..., a}_{p+1}, \underbrace{\lambda_{p+2}, ..., \lambda_{m-(p+2)}}_{m-2(p+1)}, \underbrace{b, ..., b}_{p+1}\}$$

The global interval $[a, b]$ is called the patch. A knot vector is said open if the first and last knots have multiplicity $p + 1$; in this work only non periodic open knot vectors are considered, with multiplicity equal to 1 for each internal knot, so that we have C^{p-1} parametric continuity in each patch.

If in the knot vector there aren't internal knots the basis functions reduce to the Bernstein polynomials, so that the B-Spline interpolation is a generalization of the Bezier's interpolation. An interesting property of the B-Spline interpolation of a curve with an open knot vector is that the interpolated curve is tangent to the control polygon at the ends.

The degrees of freedom of the model, i.e., the displacement $\boldsymbol{u}$ and the torsional rotation ϕ are interpolated by means of B-splines:

$$\begin{aligned} \mathbf{q}(\lambda) &= \{p_x(\lambda), p_y(\lambda), p_z(\lambda), \phi(\lambda)\} \\ p_\alpha(\lambda) &= \sum_{i=1}^{n} N_{i,p} P_{\alpha i} = \hat{\mathbb{M}}\boldsymbol{P}_\alpha \;\; \phi(\lambda) = \sum_{i=1}^{n} N_{i,p}\Phi_i = \hat{\mathbb{M}}\boldsymbol{\Phi} \end{aligned} \tag{41}$$

so that $\boldsymbol{p}(\lambda) = \mathbb{M}\boldsymbol{P}$ with

$$\mathbb{M} = \begin{bmatrix} \hat{\mathbb{M}} & 0 & 0 \\ 0 & \hat{\mathbb{M}} & 0 \\ 0 & 0 & \hat{\mathbb{M}} \end{bmatrix} \tag{42}$$

where the matrix $\hat{\mathbb{M}} = [N_{1,p}, ..., N_{n,p}]$. The first and the second derivatives of the basis functions are

$$\mathbb{B} = \frac{d\mathbb{M}}{d\lambda} \qquad \mathbb{D} = \frac{d^2\mathbb{M}}{d\lambda^2}. \tag{43}$$

while the interpolation of the second gradient along the arc-length, according to expression (21) is

$$\begin{aligned}\frac{d^2\bullet}{dS^2} &= \frac{1}{\|\boldsymbol{t}_0\|}\frac{d}{d\lambda}\left(\frac{1}{\|\boldsymbol{t}_0\|}\frac{d\bullet}{d\lambda}\right) - \frac{1}{\|\boldsymbol{t}_0\|^2}\frac{1}{\|\boldsymbol{t}\|^2}\left(\frac{d\boldsymbol{t}}{d\lambda}\cdot\boldsymbol{t}\right)\frac{d\bullet}{d\lambda} = \\ &\frac{1}{\|\boldsymbol{t}_0\|^2}\mathbb{D} - \frac{\mathbb{D}\mathbf{P}\cdot\mathbb{B}\mathbf{P}}{\|\boldsymbol{t}\|^2\|\boldsymbol{t}_0\|^2}\mathbb{B} = \mathbb{X}\end{aligned} \tag{44}$$

The cartesian components of the sectional axes $\hat{\boldsymbol{n}}, \hat{\boldsymbol{\nu}}$ are given by expressions (8), and will be indicated as

$$\boldsymbol{n} = \mathbb{N}(\mathbf{P}) \quad \boldsymbol{\nu} = \mathbb{V}(\mathbf{P}). \tag{45}$$

4.2 Material Stiffness Matrix

The material (tangent) stiffness matrix of the rod is derived from the virtual power expression (36) using the definitions (37) of the stress resultants and the constitutive equations (39) for the stress components. We have three additive contributions to the internal power.

The *axial stiffness* is obtained from the following integral, where a tilde denotes virtual deformations:

$$\int_{L_0} E\mathcal{A}\dot{\varepsilon}\tilde{\varepsilon}dS = \int_0^{L_0} E\mathcal{A}\left(\boldsymbol{t}\cdot\frac{\dot{\boldsymbol{u}}}{dS}\right)\left(\boldsymbol{t}\cdot\frac{\tilde{\boldsymbol{u}}}{dS}\right)\|\boldsymbol{t}_0\|d\lambda \tag{46}$$

Using the approximation $\boldsymbol{t} = \frac{\mathbb{B}\mathbf{P}}{\|\boldsymbol{t}_0\|}$, the axial stiffness matrix gets the form

$$K_{ax} = \begin{bmatrix} \int_0^{L_0} E\mathcal{A}\frac{\left(\mathbb{B}^T\mathbb{B}\mathbf{P}\right)^T\left(\mathbb{B}^T\mathbb{B}\mathbf{P}\right)}{\|\boldsymbol{t}_0\|^3}d\lambda & \mathbf{0} \\ \mathbf{0} & \mathbf{0} \end{bmatrix}\begin{bmatrix} \Delta\boldsymbol{P} \\ \Delta\boldsymbol{\Phi} \end{bmatrix} \tag{47}$$

Since the axes $\hat{\boldsymbol{n}}, \hat{\boldsymbol{\nu}}$ have been chosen principal of inertia, the *bending material stiffness* is obtained from the expression

$$\begin{aligned}&\int_0^{L_0} E\mathcal{I}_\nu\left(\frac{d^2\dot{\boldsymbol{u}}}{dS^2}\cdot\hat{\boldsymbol{n}} + \hat{\boldsymbol{\nu}}\cdot\frac{d\hat{\boldsymbol{t}}}{dS}\|\boldsymbol{t}\|\dot{\phi}\right)\left(\frac{d^2\tilde{\boldsymbol{u}}}{dS^2}\cdot\hat{\boldsymbol{n}} + \hat{\boldsymbol{\nu}}\cdot\frac{d\hat{\boldsymbol{t}}}{dS}\|\boldsymbol{t}\|\tilde{\phi}\right) + \\ &\int_0^{L_0} E\mathcal{I}_n\left(-\frac{d^2\dot{\boldsymbol{u}}}{dS^2}\cdot\hat{\boldsymbol{\nu}} + \hat{\boldsymbol{n}}\cdot\frac{d\hat{\boldsymbol{t}}}{dS}\|\boldsymbol{t}\|\dot{\phi}\right)\left(-\frac{d^2\tilde{\boldsymbol{u}}}{dS^2}\cdot\hat{\boldsymbol{\nu}} + \hat{\boldsymbol{n}}\cdot\frac{d\hat{\boldsymbol{t}}}{dS}\|\boldsymbol{t}\|\tilde{\phi}\right)\end{aligned} \tag{48}$$

The geometric curvatures are interpolated as follows

$$
\begin{aligned}
\hat{\boldsymbol{\nu}} \cdot \frac{d\hat{\boldsymbol{t}}}{dS}\|\boldsymbol{t}\| &= \frac{1}{\|\boldsymbol{t}_0\|}\mathbb{V}^T\left(\mathrm{I}_{3\times 3} - \frac{\mathbb{B}\mathbf{P}\otimes\mathbb{B}\mathbf{P}}{\|\boldsymbol{t}\|^2}\right)\mathbb{D}\mathbf{P} = \rho_\nu \\
\hat{\boldsymbol{n}} \cdot \frac{d\hat{\boldsymbol{t}}}{dS}\|\boldsymbol{t}\| &= \frac{1}{\|\boldsymbol{t}_0\|}\mathbb{N}^T\left(\mathrm{I}_{3\times 3} - \frac{\mathbb{B}\mathbf{P}\otimes\mathbb{B}\mathbf{P}}{\|\boldsymbol{t}\|^2}\right)\mathbb{D}\mathbf{P} = \rho_n
\end{aligned}
\tag{49}
$$

The material bending stiffness is therefore given by the sum of the two matrices:

$$
K_{\hat{n}} = E\mathcal{I}_\nu \int_0^{L_0} \begin{bmatrix} \mathbb{X}^T\mathbb{N}\mathbb{N}^T\mathbb{X} & \rho_\nu\mathbb{X}^T\mathbb{N}\hat{\mathbb{M}} \\ \rho_\nu\hat{\mathbb{M}}^T\mathbb{N}^T\mathbb{X} & \rho_\nu^2\hat{\mathbb{M}}^T\hat{\mathbb{M}} \end{bmatrix} \begin{bmatrix} \Delta\boldsymbol{P} \\ \Delta\boldsymbol{\Phi} \end{bmatrix} \tag{50}
$$

$$
K_{\hat{\nu}} = E\mathcal{I}_n \int_0^{L_0} \begin{bmatrix} \mathbb{X}^T\mathbb{V}\mathbb{V}^T\mathbb{X} & -\rho_n\mathbb{X}^T\mathbb{V}\hat{\mathbb{M}} \\ -\rho_n\hat{\mathbb{M}}^T\mathbb{V}^T\mathbb{X} & \rho_n^2\hat{\mathbb{M}}^T\hat{\mathbb{M}} \end{bmatrix} \begin{bmatrix} \Delta\boldsymbol{P} \\ \Delta\boldsymbol{\Phi} \end{bmatrix} \tag{51}
$$

The torsional internal power is

$$
\int_0^{L_0} G\mathcal{J}\dot{\chi}_t\tilde{\chi}_t\|\boldsymbol{t}_0\|d\lambda \tag{52}
$$

The interpolation of the torsional velocity of curvature is

$$
\begin{aligned}
&\frac{1}{\|\boldsymbol{t}\|}\left(\hat{\boldsymbol{t}} \times \frac{d\hat{\boldsymbol{t}}}{dS}\right)\cdot\frac{d\dot{\boldsymbol{u}}}{dS} + \frac{d\dot{\phi}}{dS} = \frac{1}{\|\boldsymbol{t}\|}\left(-\hat{\boldsymbol{\nu}}\cdot\frac{d\hat{\boldsymbol{t}}}{dS}\frac{d\dot{\boldsymbol{u}}}{dS}\cdot\hat{\boldsymbol{n}} + \hat{\boldsymbol{n}}\cdot\frac{d\hat{\boldsymbol{t}}}{dS}\frac{d\dot{\boldsymbol{u}}}{dS}\cdot\hat{\boldsymbol{\nu}}\right) + \frac{d\dot{\phi}}{dS} \\
&= \frac{1}{\|\boldsymbol{t}_0\|}\frac{1}{\|\boldsymbol{t}\|^2}\left(-\rho_\nu\mathbb{N}^T + \rho_n\mathbb{V}^T\right)\mathbb{B}\dot{\boldsymbol{P}} + \frac{1}{\|\boldsymbol{t}_0\|}\hat{\mathbb{B}}\dot{\boldsymbol{\Phi}} = \frac{1}{\|\boldsymbol{t}_0\|}\mathbb{X}_t\dot{\boldsymbol{P}} + \frac{1}{\|\boldsymbol{t}_0\|}\hat{\mathbb{B}}\dot{\boldsymbol{\Phi}}.
\end{aligned}
\tag{53}
$$

The *torsional stiffness matrix* is therefore

$$
K_t = G\mathcal{J}\int_0^{L_0}\frac{1}{\|\boldsymbol{t}_0\|^2}\begin{bmatrix} \mathbb{X}_t^T\mathbb{X}_t & \mathbb{X}_t^T\hat{\mathbb{B}} \\ \hat{\mathbb{B}}^T\mathbb{X}_t & \hat{\mathbb{B}}^T\hat{\mathbb{B}} \end{bmatrix}\begin{bmatrix} \Delta\boldsymbol{P} \\ \Delta\boldsymbol{\Phi} \end{bmatrix} \tag{54}
$$

As it is evident, the degrees of freedom are the displacements of the control point, and their torsional rotations. Rotations about the normal axes are not included in the model, and are calculated according to equations (17). From their construction, it can be seen that only the first two B-spline bases have non vanishing derivative at the first end (resp. only the last two at the second end), so that a boundary condition on the rotation only affects the position of the first two control points. Indeed, in the case the end point of the beam is fixed, so that the first control point doesn't move, the zero rotation condition requires that the normal components of the velocity of the second control point be zero.

5 Multi-patch analysis

Let's examine the simplest case of a single beam that we wish to divide in many patches. Concentrated loads may be applied at the joints. The general case of beams matching with different orientation at the joints can be treated in a similar way.

We assume that the initial positioning of the patches satisfy parametric C^1 continuity at the joints, that guarantees that the tangent vector $\boldsymbol{t}$ is everywhere continuous, in direction and norm. The last two control points of the adjoint patches are so aligned, and their distance from the joint is the same. This can be obtained in several ways, and will not be discussed here.

The scheme discussed in the previous sections can not be applied directly to the case of a multipatch beam. Indeed, since, as has been observed, only the displacements are used as degrees of freedom, rotations around the normal axes at the joints are not constrained, so that a kinematically undetermined structure is obtained, leading to a singular stiffness matrix after assemblage. Additional constraints have to be enforced, specifically, the continuity of the rotations ω_n, ω_ν. Recalling expressions (17), the continuity requires that both $\|\boldsymbol{t}\|$ and the normal components of the velocity gradient, $\frac{d\boldsymbol{u}}{dS} \cdot \hat{\boldsymbol{n}} = \dot{\boldsymbol{t}} \cdot \hat{\boldsymbol{n}}$, $\frac{d\boldsymbol{u}}{dS} \cdot \hat{\boldsymbol{\nu}} = \dot{\boldsymbol{t}} \cdot \hat{\boldsymbol{\nu}}$ be continuous. Since

$$\dot{\overline{\|\boldsymbol{t}\|}} = \dot{\boldsymbol{t}} \cdot \hat{\boldsymbol{t}} \tag{55}$$

interpatch continuity is ensured imposing the continuity of the tangent vector $\boldsymbol{t}$, or, numerically, $\mathbb{B}\boldsymbol{P}^+ = \mathbb{B}\boldsymbol{P}^-$, since the initial tangent is assumed to be continuous within numerical errors. However, it is noticed that the term (55) is also equal to $\|\boldsymbol{t}\|\varepsilon$, so, if the initial tangent vector is assumed to be continuous, the continuity of the tangent norm is implied by the equilibrium equations enforced with the stiffness matrix. Therefore it is sufficient to add as constraint the continuity of the normal components of the velocity of the tangent,

$$[\![\dot{\boldsymbol{t}} \cdot \hat{\boldsymbol{n}}]\!] = 0 \quad [\![\dot{\boldsymbol{t}} \cdot \hat{\boldsymbol{\nu}}]\!] = 0 \tag{56}$$

The continuity of the tangent component of the gradient of the velocity can in any case be enforced as supplementary constraint in order to minimize the numerical errors.

6 Examples

6.1 Bezier's multipatch pretwisted beam

The first example concerns a benchmark proposed by McNeal [15] on a pretwisted cantilever, with linear variation of the twist angle, with two loading conditions, see figures 2(a), 2(b). The data are $L = 12$, $E = 29 * 10^6$, $h_n = 1.1$, $h_\nu = 0.32$ $\phi(S) = \frac{\pi}{2}\frac{\lambda}{L}$, with $\lambda \in [0, 1]$.

In figures 2(c), 2(d) is reported the convergence of the error of the tip displacements dual of the applied load with respect to the exact value for increasing number of patches (in these figures as well as in the following, on the abscissa is reported the number of degrees of freedom, function of the number of patches. For each patch a Bezier interpolation is used). The convergence rate is function of the degree of the polynomial interpolation, as happens with single patch isogeometric models. No influence of the reduced interpatch continuity appears in this example, since the initial (continuous) tangent vectors are not affected by the deformation process.

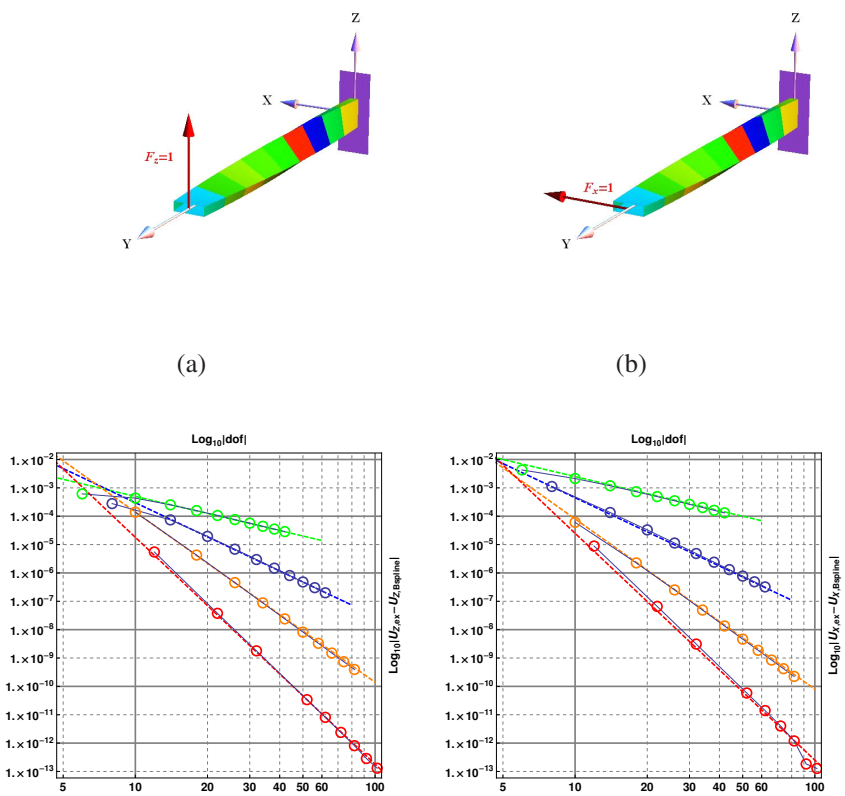

(a) (b)

(c) (d)

Figure 2: 3D cantilever pre-twisted beam; 2(a) initial geometry load case-1;2(b) initial geometry load case-2; 2(c) convergence's error for the $u_z(L)$ at the free end; 2(d) convergence's error for the $u_x(L)$ at the free end (p=2 green, p=3 blue, p=4 orange, and p=5 red, p is the polynomial degree).

6.2 Bezier's multipatch 3D-cantilever arch with a point force

The next example concerns a geodetic horizontal arch loaded at the tip by a vertical force $\boldsymbol{F} = \{0, 0, -1\}, [kN]$. The radius of the centroid curve is $R = 1\,[m]$ the section is rectangular with $h_n = 0.1$ and $h_\nu = 0.01\,[m]$ respectively, and $E =$

$1.999 * 10^8\,[kN/m^2]$, figure 3(a). Figures 3(b) and subsequent show the convergence error on the tip displacement and rotation, and for the bending moment, twisting moment and shear force at the constrained end. It is interesting to note that while for few patches the convergence rate is equal to the splines degree p, as in the case of single patch analysis, for larger number of patches the convergence rate becomes smaller, tending to $p-1$.

6.3 Bezier's multipatch 2D-cantilever arch with a couple

$R = 1\,[m]$, $h_n = 0.1\,[m]$, $h_\nu = 0.01\,[m]$, $E = 1.999 * 10^8\,[KN/m^2]$. In figure-7 we consider the influence of the slenderness ratio R/h on the solution for a couple $M_h = \left(\frac{h}{R}\right)^3$ applied at the tip. in this manner the vertical displacement for different value of M_h is h-independent, so that the horizontal line represent the exact solution for different M_h values. The example shows the existence of locking phenomena in the isogeometric interpolation. However the energy converges to the exact value (figure 6(b)).

6.4 Bezier's multipatch 2D-cantilever arch with a point force

$R = 1\,[m]$, $h_n = 0.1\,[m]$, $h_\nu = 0.01\,[m]$, $E = 1.999 * 10^8\,[KN/m^2]$. In figure-6.4 we consider the influence of the slenderness ratio $\frac{R}{h}$ on the vertical displacement of the free end, for a fixed number of degree of freedom and for a fixed $F = 1\,[KN]$. Again a kind of locking is observed.

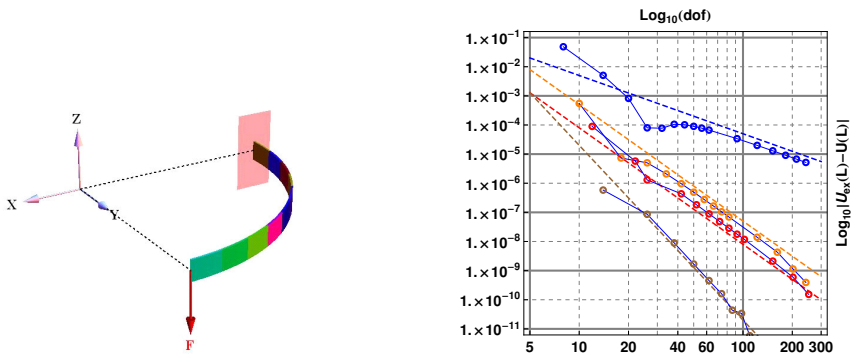

(a) (b)

Figure 3: 3D cantilever arch with a point force at the end; 3(a) initial geometry, 3(b) convergence's error for the vertical displacement at the free end $u_z(L)$, for $R/h_n = 100$ (p=2 green, p=3 blue, p=4 orange, p=5 red, and p=6 brown, p is the polynomial degree).

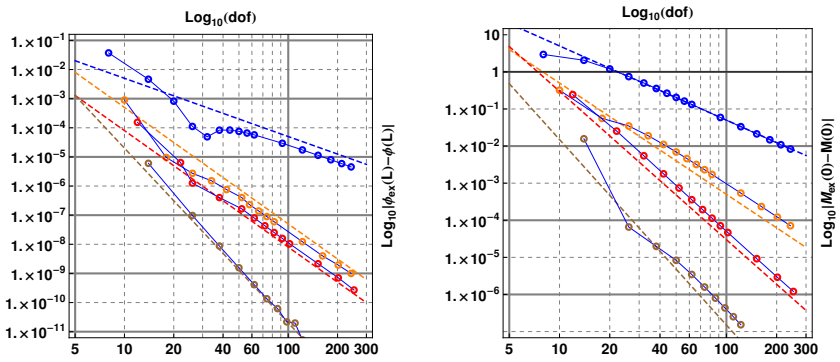

(a) (b)

Figure 4: Figure-4(a) error's convergence for the free end rotation $\phi(L)$, Figure-4(b) error's convergence for the bending moment at the constrained end, for $R/h_n = 100$ (p=2 green, p=3 blue, p=4 orange, p=5 red, and p=6 brown, p is the polynomial degree).

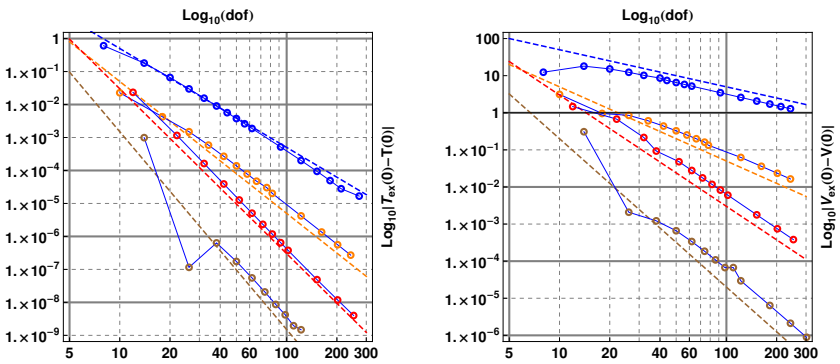

(a) (b)

Figure 5: Figure-5(a) error's convergence for the twisting moment at the constrained end, Figure-5(b) error's convergence for the shear force at the constrained end, for $R/h_n = 100$ (p=2 green, p=3 blue, p=4 orange, p=5 red, and p=6 brown, p is the polynomial degree).

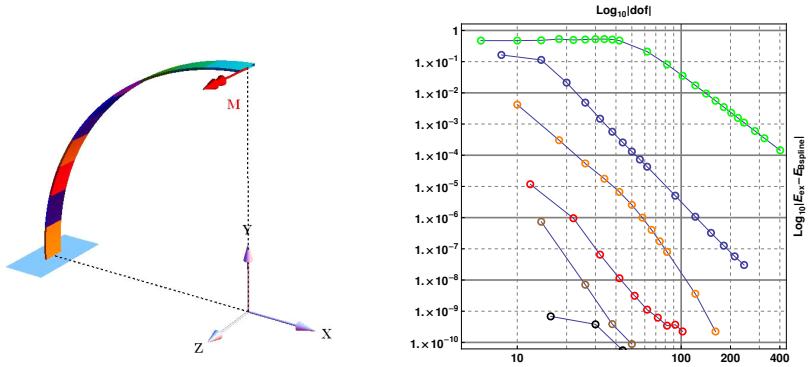

(a) (b)

Figure 6: 3D cantilever arch with a couple at the end; 6(a) initial geometry, 6(b) convergence's error in energy, for $R/h_n = 100$ (p=2 green, p=3 blue, p=4 orange, p=5 red, p=6 brown and p=7 black, p is the polynomial degree).

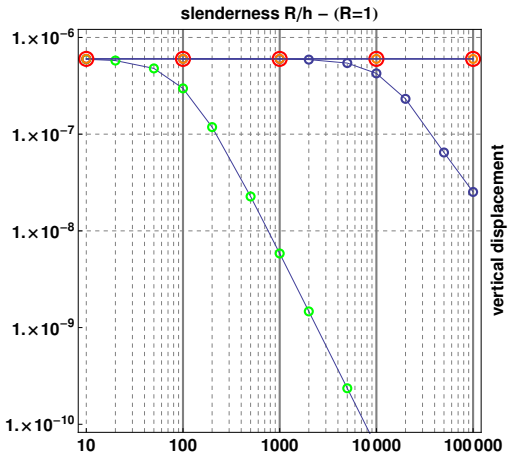

Figure 7: Influence of the slenderness ratio on the vertical displacement of the free end, (p=2 green, p=3 blue, p=4 orange, p=5 red, p is the polynomial degree).

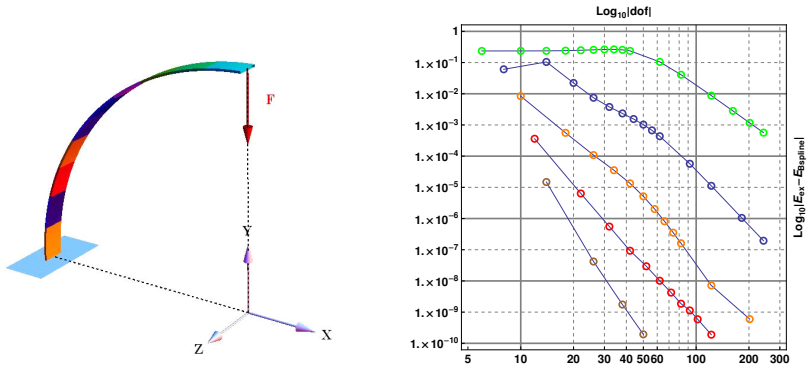

(a) (b)

Figure 8: 2D cantilever arch with a point force at the end; 8(a) initial geometry, 8(b) convergence's error in energy, for $R/h_n = 100$ (p=2 green, p=3 blue, p=4 orange, p=5 red, and p=6 brown, p is the polynomial degree).

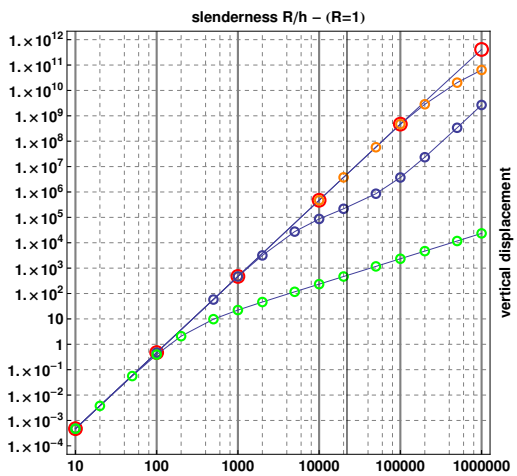

Figure 9: Influence of the slenderness ratio on the vertical displacement of the free end, (p=2 green, p=3 blue, p=4 orange, p=5 red, p is the polynomial degree).

7 Conclusions

The main findings of the paper are as follows:

- a model for Kirchhoff-Lovespace rods has been presented, that employs as degrees of freedom the position vector of the point of the rod axis and the torsional rotation around the current tangent;

- the model has been implemented in a numerical scheme based on B-splines interpolation;

- two strategies have been compared, one that employs a single patch for the whole rod, and the other that employs a multiple patch discretization with C^1 geometric continuity at the joints;

- convergence analyses have been carried out on a number of examples, which have shown that with single patch interpolation the rate of convergence equals the degree p of the B-splines, while with multiple patches the rate of convergence at most reaches $p - 1$.

In addition, some preliminary results on membrane locking have been presented, that will be object of future works.

References

[1] A. Goriely, M. Nizette and M. Tabor. On the dynamic of elastic strips. *J. Nonlinear Sci.*, **11**, 3–45, 2001.

[2] J. Langer and D.A. Singer. Lagrangian aspects of the kirchhoff elastic rod. *SIAM REVIEW*, **38**, 605–618, 1995.

[3] S. S. Antman. *Nonlinear problem of elasticity*. Springer-Verlag, New York, 1995.

[4] J. C. Simo and L. Vu-Quoc. A three dimensional finite strain rod model. part ii: computational aspect. *Comput. Methods. Appl. Mech. Engrg.*, **58**, 79–116, 1986.

[5] M. A. Crisfield. A consistent co-rotational formulation for non-linear, three-dimensional, beam elements. *Comput. Methods Appl. Mech. Engrg.*, **81**, 131–150, 1990.

[6] G. Becker and L. Noels. A fracture framework for euler-bernouilli beams based on a full discontinuous galerkin formulation/extrinsic cohesive law combination. *Int. J. Numer. Meth. Engrg.*, **85**, 1227–1251, 2011.

[7] D.J. Benson, Y. Bazilevs, M.C. Hsu and T.J.R. Hughes. A large deformation, rotation-free, isogeometric shell. *Comput. Methods Appl. Mech. Engrg.*, (200), 1367–1378, 2011.

[8] D.J. Benson, Y. Bazilevs, M.C. Hsu and T.J.R. Hughes. Isogeometric shell analysis: The reissner-mindlin shell. *Comput. Methods Appl. Mech. Engrg.*, (199), 276–289, 2010.

[9] J. Kiendl, K.-U. Bletzinger, J. Linhard and R. Wuchner. Isogeometric shell analysis with kirchoff-love elements. *Comput. Methods Appl. Mech. Engrg.*, **189**, 3902–3914, 2009.

[10] J. Kiendl, Y.Bazilevs, M.-C. Hsu, R. Wuchner and K.-U. Bletzinger. The bending strip method for isogeometric analysis of kirchhoff-love shell structures comprised of multiple patches. *Comput. Methods Appl. Mech. Engrg.*, **199**, 2403–2416, 2010.

[11] J.C. Simo. A three dimensional finite strain rod model. part ii, computational aspects. *Compt. Methods Appl. Mech. Engrg.*, **58**, 79–116, 1986.

[12] C. Gontier and C. Vollmer. A large displacement analysis of beam using a cad geometric definition. *Computer and Structure*, **57**(6), 981–989, 1995.

[13] R. Echter and M. Bischoff. Numerical efficiency, locking and unlocking of nurbs finite elements. *Comput. Methods Appl. Mech. Engrg.*, **199**, 374–382, 2010.

[14] M. Cuomo L. Greco. B-spline interpolation of kirchhoff-love space rods. *Comput. Methods Appl. Mech. Engrg.*, **submitted to**, 2012.

[15] R.H McNeal and R.L. Harder. A proposed standard set of ptoblems to test finite elements accuracy. *FE Analysis and Design*, **1**, 3–20, 1985.